HIGH-RESOLUTION STELLAR VIDICON SPECTROPHOTOMETRY. I. VARIABLE MASS LOSS FROM ARCTURUS AND THE HYPOTHESIS OF GIANT CONVECTIVE ELEMENTS

H. Y. Chiu* and P. J. Adams*†
Goddard Institute for Space Studies, New York

J. L. Linsky*‡ and G. S. Basri*
Joint Institute for Laboratory Astrophysics,
National Bureau of Standards and University of Colorado, Boulder

AND

S. P. Maran* and R. W. Hobbs*
Laboratory for Solar Physics and Astrophysics,
NASA-Goddard Space Flight Center, Greenbelt
Received 1975 December 22; revised 1976 May 21

ABSTRACT

High-resolution spectrophotometry of the variable Ca II K-line in the K2 IIIp star α Boo was performed on five occasions over the period 1974 April–1976 February with the McMath Solar Telescope at Kitt Peak National Observatory and an experimental SEC vidicon camera. The results are compared with *Copernicus* observations of the Mg II h and k lines (1973 May 19; 1974 May 20) and with earlier Ca II data of Griffin, and it is found that either of two states may typically occur in the Arcturus chromosphere. From comparison with the results of model calculations for expanding chromospheres, it is concluded that these correspond respectively to a "normal" state in which the mass loss $dM/dt < 10^{-9}\ M_\odot\ \mathrm{yr}^{-1}$ and an "abnormal" state in which $dM/dt \approx 8 \times 10^{-9}\ M_\odot\ \mathrm{yr}^{-1}$. In the latter case, the expansion velocity is $\sim 13\ \mathrm{km\ s}^{-1}$ at optical depth unity in the K-line, which exceeds the local sound speed. It is suggested that the abnormal state represents the rise to the photosphere of a very large convective element ($d \sim r_*$) as hypothesized for red giants by Schwarzschild.

Subject headings: Ca II emission — stars: individual — stars: late-type — stars: mass loss — stars: chromospheres

I. INTRODUCTION

An integrating vidicon camera, previously used as a panoramic detector for nebular (Gull *et al.* 1973) and extragalactic (Chiu *et al.* 1973) observations, has been modified and applied to high dispersion stellar spectroscopy (Chiu 1976). The SEC vidicon camera, developed at the Goddard Institute for Space Studies with cooperation of the Laboratory for Solar Physics and Astrophysics, NASA–Goddard Space Flight Center, was mounted at the photographic port of the vertical spectrograph (Pierce 1964) at the 60 inch (1.5 m) McMath solar telescope of Kitt Peak National Observatory.

Livingston and Lynds (1964) first demonstrated the potential of the KPNO vertical spectrograph for high-resolution stellar observations. They employed an electronic image intensifier tube. More recently, Fahlman *et al.* (1974) searched for stellar Zeeman shifts with this apparatus, employing a refrigerated Isocon camera.

We believe that an integrating television camera is well suited to many problems in high-dispersion spectroscopy because it avoids the difficulties associated with duty cycle and possible seeing, guiding, and transparency variations that can affect scanning spectrometers; it offers higher quantum efficiency than do photographic plates; and it provides an output signal in machine-readable form, unlike the image intensifier. Lower-dispersion spectroscopy by video techniques has been practiced extensively by the Princeton group (Lowrance *et al.* 1972; Morton and Morton 1972; Morton and Richstone 1973), who have observed quasars at 9 Å mm^{-1} (resolution about 0.7 Å) at the coudé focus of the Hale reflector with an SEC vidicon system. Among other work in this field is that of the University of British Columbia group (Buchholz *et al.* 1973), who published 0.5 Å resolution stellar data taken with a silicon diode vidicon camera.

We recently initiated a program to record chromospheric diagnostics (the H- and K-lines of Ca II and the CN structure near the band head at 3883 Å) in a sample of stars of all luminosity classes in spectral types A through M. This is a preliminary report on the performance of the NASA-Goddard vidicon system. Here we report on several interesting observations of the K2 IIIp giant Arcturus (α Boo). In subsequent papers in this series we will report on and interpret data relevant to a number of questions concerning A–M stars,

including the properties of stellar chromospheres and photospheres, mass loss, and circumstellar envelopes.

The desirability of monitoring the short-term changes in the central emission features of the H- and K-lines in Arcturus by means of calibrated high-dispersion spectroscopy was suggested by Griffin (1963). He found that such changes (on time scales of days to years) were common in a collection of nearly 80 Mount Wilson spectrograms, mostly consisting of uncalibrated plates taken in radial velocities studies, and he recognized the effect as evidence for the existence of an active chromosphere in Arcturus. Liller (1968) confirmed through photoelectric monitoring that variations in the intensities of K_{2r} and K_{2v} occur even on time scales of hours. There is no clear evidence for periodicity in the data, such as might result from stellar rotation or a "stellar activity" cycle, and indeed it is possible that the spin period of Arcturus is several tens of years, with any stellar activity cycle hypothesized by scaling from that of the Sun being proportionately much longer.

II. INSTRUMENTATION

The instrumentation and its operation are described in more detail elsewhere (Chiu 1976), but we summarize the important aspects here. The detector in the present system is a magnetically focused and deflected SEC vidicon (Westinghouse 31958) with an S–20 photocathode. The 1 inch (2.54 cm) vidicon target is scanned in a 740-line raster pattern. Each line of the scan is sampled at 1024 locations with an individual pixel dwell time of 16.7 μms, chosen as a suitable compromise between the effects of Johnson noise and shot noise. The operational cycle of the vidicon camera, consisting of target erasure, target preparation, exposure, and data readout, is controlled by a hard-wired automatic sequencer. This cycle has a total duration of 2 minutes plus exposure time.

The measured noise level in operation at the telescope corresponds to about 500 electrons per pixel at 20 kHz. The preamplifier noise, with a target gain between 50 and 100, is equivalent to 5 to 10 photoelectrons per pixel. As the usual storage capacity of the target is typically less than 2000 photoelectrons per pixel, the system is effectively photon-noise limited in most applications. The photocathode is cooled to a temperature of slightly less than $0°$ C by means of a directed stream of cool N_2 gas obtained from a Dewar of liquid N_2; this reduces thermal noise to negligible levels even for exposures of several hours.

Our vidicon observing programs require very high spectral resolution, approaching that commonly used in solar spectroscopy. Our present goal is 40 mÅ, full width at half-maximum (FWHM) equivalent to 2 Å mm^{-1} dispersion with photographic detection. To achieve this spectral resolution we are using the Kitt Peak solar telescope (60 inch aperture) and spectrograph with 11 mm Å^{-1} dispersion in the seventh order single-pass mode. Even at this dispersion, high resolution requires a small entrance slit. We therefore employ a Bowen-type image slicer with entrance aperture

2×2 mm, corresponding to $5'' \times 5''$ on the sky. The image slicer defines an entrance slit of 270 μm $\times$ 2 cm and thus a theoretical spectral resolution element (FWHM) of 25 mÅ which corresponds spatially to 270 μm ($\parallel$) and 2 cm ($\perp$) with respect to the dispersion at the exit plane of the spectrograph. Since the vidicon horizontal scan lines are along the dispersion, the vidicon pixel size is, by comparison, 25 μm ($\parallel$) and approximately 35 μm ($\perp$) with respect to the dispersion direction.

In order to use the vidicon system most efficiently, we have built an anamorphic lens system to reduce the spectrum format. Since the signal-to-noise ratio in each scan is nominally 30, we feel that the sum of about 14 scan lines covering the entire height of the spectrum should give satisfactory signal-to-noise at the bottom of strong absorption lines. The transfer lens system accomplishes this by a factor of 43 reduction perpendicular to the dispersion direction. Since only 14 scan lines are used for the spectrum, there is considerable flexibility in choice of the best section of the photocathode in terms of uniformity of response and other characteristics.

Along the dispersion, 10 cm of spectrum are reduced a factor of 5 to 2 cm on the photocathode, or 2.0 pixels per spectral resolution element. This reduction factor is not optimal, but was chosen as a compromise between resolution and usable spectral range (about 9 Å at the K-line).

The design of the transfer lens system has evolved considerably during the progress of our work. The final optical system consists of one negative cylindrical lens of focal length -4.7 cm, a spherical lens system (Nikon f:2; 5 cm focal length), and a semicylindrical lens of focal length 1 cm, as shown in Figure 1. Focusing is achieved in directions perpendicular and parallel to dispersion. The final beam emerges with anisotropic focal ratios; in the direction perpendicular to dispersion an equivalent focal ratio of around f:1.4 is achieved, while in the direction along dispersion the equivalent focal ratio is f:12. We have performed a ray trace calculation to determine the characteristics of the optics; in our current system, using a simple cylindrical lens, the line of confusion along the perpendicular direction for the outermost ray from the telescope is roughly equal to the design height (0.5 mm) and this calculation is confirmed by experimental data. It appears that the design is close to optimum.

We have tested the spectral resolution of the system at the telescope by observing a laser line and a thorium lamp with the telescope in autocollimation and by recording the solar CN band-head region near 3883 Å. The laser line exhibits a full width at half-maximum (FWHM) of 4 to 5 pixels, corresponding to 50 to 62 mÅ. In the thorium lamp spectrum we were able to resolve two lines 50 mÅ apart. The solar CN band-head spectrum is perhaps the most realistic test of resolution because it exhibits a wide range of line depths and separations. In Figure 2 our observed single-pass solar spectrum is compared with the double-pass, higher-resolution (~ 24 mÅ) spectrum in the *Kitt Peak Solar Atlas* (Brault and Testerman 1972).
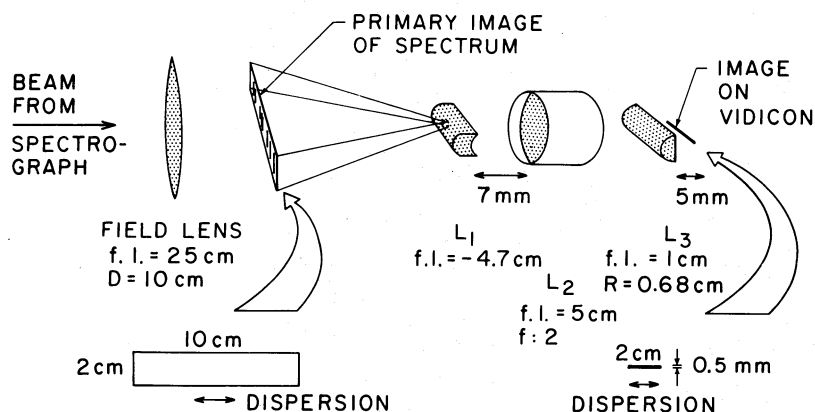
FIG. 1.—Schematic for the cylindrical transfer lens system. L_1 is a negative cylindrical lens of focal length -4.7 cm, L_2 is an f:2.5 cm Nikon spherical lens system, and L_3 is half a cylindrical lens. In order to bring both horizontal and vertical images to the same focal plane, it is necessary to use a pair of negative and positive cylindrical lenses. The distance between L_1 and L_2 is around 7 cm but not critical, and focusing of the horizontal and vertical images is achieved by varying the separation between L_2 and L_3. The final image is about 5 mm behind the last lens surface.
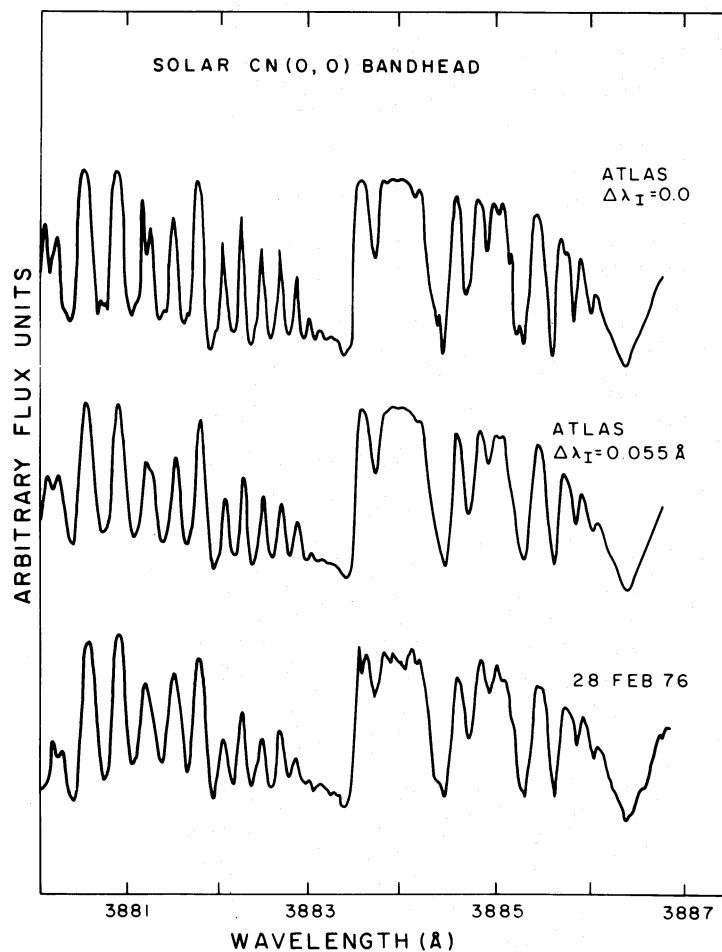

FIG. 2.—Spectra of the solar CN (0, 0) band head near $\lambda3883$ Å. *Top*, double-pass spectrum from Brault and Testerman (1972). *Middle*, same spectrum but convolved with an assumed Gaussian instrumental profile with a full width at half-maximum of 55 mÅ. *Bottom*, single-pass spectrum observed with the same spectrograph and SEC vidicon system on 1976 February 28. Additional noise between 3883.5 and 3884.2 Å is due to saturation.

We also performed a number of numerical experiments in which the Atlas spectrum was convolved with assumed Gaussian instrumental profiles of different half-widths. The best match (FWHM = 55 mÅ) is also shown in Figure 2.

III. DATA PROCESSING

Each spectrum represents a one-dimensional data string, but considerable redundancy exists because the spectrum is collected in a two-dimensional format with ~14 scan lines. After removal of dark current, differential photocathode sensitivity, and storage grid saturation effects, this redundancy is utilized to enhance the signal-to-noise ratio of the spectrum by simple averaging of the scan lines. We align the scan lines parallel to the spectral dispersion to average out random zero-level shifts between successive lines. Any remaining noise is minimized by appropriate filtering.

A block outline of the data reduction process is shown in Figure 3. The Ⓜ characters represent manual interaction with the data. In more recent work we have begun to eliminate these interactions since they are extremely time consuming. The Ⓕ characters represent the application of noise filtering techniques to the data.

The initial part of any data reduction process is to separate data from nondata. For spectra, considerable savings in storage space and processing time are achieved by determining the limits of each spectrum within its much larger digitized readout array and retaining only that part of the array containing the spectrum. In principle this needs to be done for only one spectrum each night, since all spectra should fall on the same part of the photocathode. However, insertion and removal of filters at the telescope can cause spectrum shifts of up to 20 scan lines during a night's observations at different wavelengths (such shifts are precisely calibrated as part of the observational process).

The response curve for the SEC vidicon tube is linear for low signal levels but saturates for high signal levels. We find the response curve to be approximated accurately by a hyperbolic tangent function. In order to correct the data for saturation effects, we must first determine the true zero level of the data and the saturation level for each part of the photocathode containing data.

The saturation levels of the photocathode are readily obtained from a short (~3 min) saturated exposure of a radiometric standard lamp with the telescope in autocollimation. We usually determine the true zero level of the data by taking a zero exposure frame before and after each long time exposure ($\geqslant 30$ min). However, for minimal dark current exposures ($\leqslant 30$ min) that part of the digital data array not containing the spectrum can be used to determine the true zero level for each frame.

Prior to removal of saturation effects it is important to perform noise filtering to ensure that no signal in the data array is near or above the saturation level.
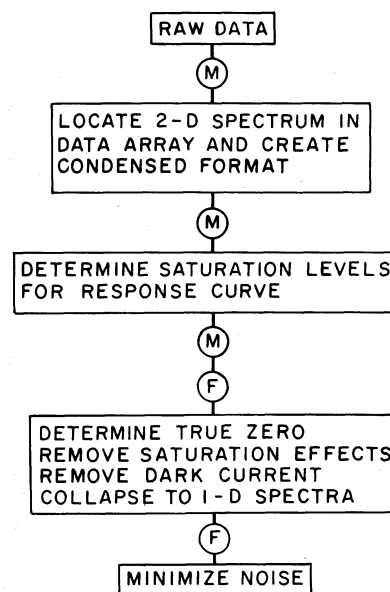

FIG. 3.—Flow chart of the vidicon data reduction process.

(A signal in the data array can be greater than the saturation level if there happens to be a blemish in the corresponding location of the vidicon storage grid.) Statistical noise peaks superposed on a strong noise-free signal can approach so closely to the saturation level that inversion of the hyperbolic tangent scales the noise disproportionately. This is eliminated by clipping the signal if it is larger than 0.9 times the saturation level. In our current observational material, this situation is only serious for blemishes (which are unwanted anyway) and for the peaks of the CN molecular bands which are not needed in detail. In all other situations where clipping is necessary, the signal is already greatly overexposed and thus worthless. (It also should be mentioned that the typical signal is too weak, rather than too strong!)

After correction for saturation effects, we remove the dark current by subtracting a simple linear interpolation between the signals on two smoothed strips of the digital array on either side of the spectrum. This is done at each wavelength. In the present work these strips have been selected manually for each spectrum in order to exclude blemishes.

Up to this point the spectra are still in their original two-dimensional format. Collapse to a one-dimensional format is done by averaging those scan lines containing the spectrum. Typically this enhances the signal-to-noise ratio by a factor of ~4. Since blemishes or bad sections of target may appear in any given scan line despite efforts to use the best section of the vidicon tube, spurious signals may appear in a spectrum. These spurious signals are reproducible in location and thus are easily removed. The resulting spectra are then smoothed by either a simple smoothing filter or a more complex Fourier transform filter, whichever appears more reliable.
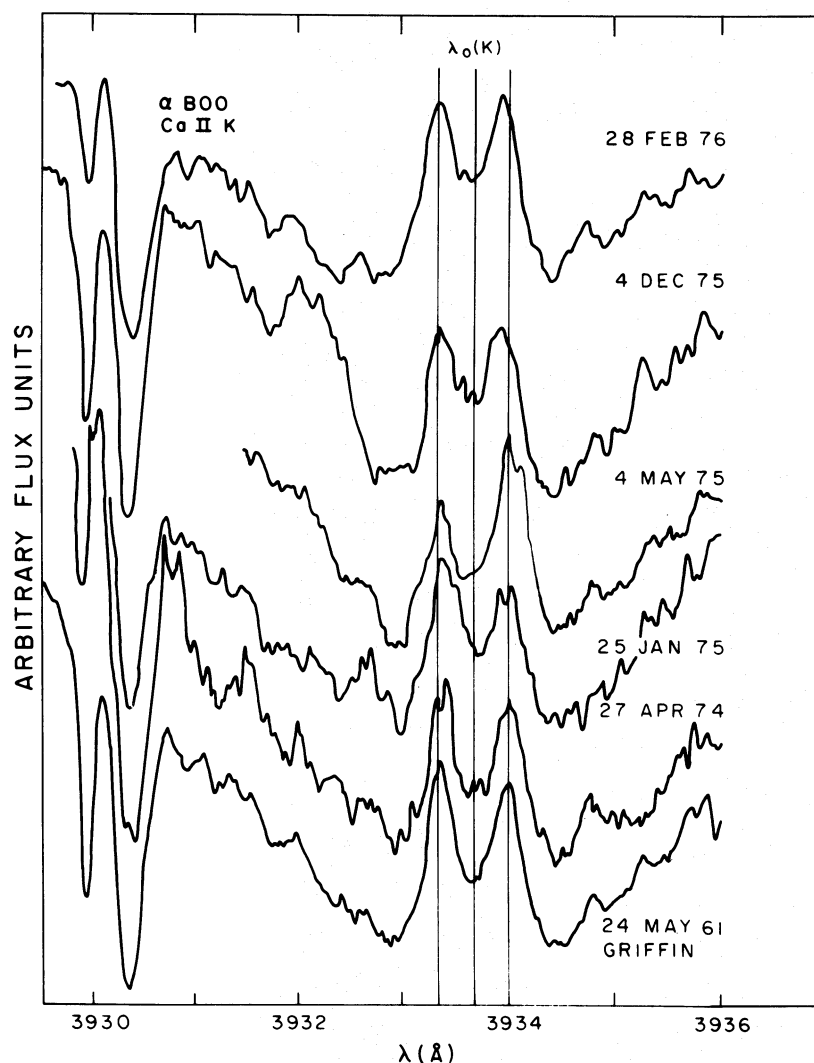
FIG. 4.—Profiles of the Ca II K line in Arcturus obtained on various dates during 1974–1976, as indicated. The wavelength scale is obtained from observations of a thorium lamp or of Vega on the same night. Also given is the profile obtained by Griffin (1968) on 1961 May 24.

IV. OBSERVATIONS OF THE K LINE IN ARCTURUS

We have observed the K-line of Arcturus on five occasions: 1974 April 27, 1975 January 25, 1975 May 4, 1975 December 4, and 1976 February 28. These profiles are given in Figure 4 together with the profile obtained by Griffin (1968) on 1961 May 24. The wavelength scale for our data is established by observations of a thorium lamp or the Vega K-line on the same night and corrections for the relative radial velocities of the two stars and the components of the Earth's orbital motion toward the two stars. The spectral resolution of the early data is about 96 mÅ but was improved to 55 mÅ in the last set of data (see § II) thanks to improvements in the optical adjustment procedures. The 1976 February 28 profile has comparable signal-to-noise to the Griffin profile yet was obtained in 15 minutes with a 53 inch[1] (1.3 m) aperture telescope compared to 125 minutes with an 100 inch (2.5 m) aperture for the Griffin profile. The increase in speed of the SEC vidicon system over Griffin's film would thus be a factor of 30 if the two spectrographs had comparable efficiencies. In fact, the KPNO vertical spectrograph does not have a very good grating and was not designed for stellar work.

We note that in Figure 4 the Arcturus K-line typically appears nearly symmetric, with the blue emission peak equal to or brighter than the red emission peak. The 1975 May 4 profile, however, is qualitatively different, with the red peak brighter than the blue peak and the K_3 central absorption feature shifted 20 ± 5 km s^{-1}

---

[1] Owing to the heliostat mounting of this telescope, the projected aperture is 53 instead of 60 inches for Arcturus.
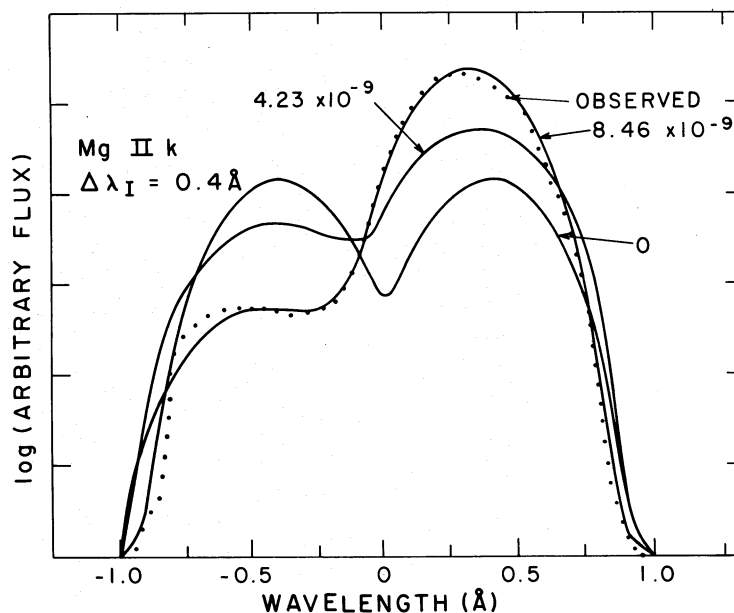
Fig. 5.—Computed Mg II k line profiles from Fig. 7, but smoothed to the *Copernicus* V2 channel instrumental resolution of 0.4 Å. Filled circles indicate the *Copernicus* observations of Moos *et al.* (1974).

to the blue with respect to rest line center at the stellar radial velocity.

While changes in the K-line profile shape have been previously noted by Griffin (1963) and Liller (1968), we feel it important to discuss these changes because of recent correlative *Copernicus* observations and developments in interpretative diagnostics. Hereafter, we refer to the quasi-symmetric profile with blue peak slightly brighter than the red peak as the "normal" profile and the asymmetric profile with red peak brighter than blue peak and K_3 shifted to the blue as the "abnormal" profile. The 1975 May 4 profile is an example of an abnormal profile. Our limited data suggest that the normal profile is more common.

In Figure 5 are *Copernicus* observations of the Arcturus Mg II h and k resonance lines, analogous to Ca II H- and K-lines, as obtained by Moos *et al.* (1974) on 1973 May 19. Despite their low spectral resolution of 0.4 Å these profiles are clearly similar to the abnormal Ca II profiles, and the asymmetry cannot be explained by interstellar absorption (McClintock *et al.*

1975). Subsequent unpublished low-resolution and high-resolution observations on 1974 May 20 with *Copernicus* show similar abnormal profiles with k_3 minima shifted 20 km s^{-1} shortward. We summarize these data in Table 1.

V. MASS LOSS CALCULATION

The observed abnormal Ca II and Mg II profiles can be readily explained by postulating an expanding chromosphere and loss of mass from the star. For a static atmosphere a symmetric, double emission-peaked profile such as the "normal" Ca II and Mg II resonance line profiles (defined in the previous section) is a natural consequence of a chromospheric rise in temperature, a collisionally dominated source function, and chromospheric line optical depths that are greater than the thermalization length (cf. Mihalas 1970). Ayres and Linsky (1975) have shown that the observed intensities and self-reversals of the Ca II K- and Mg II k-lines and the normal profile of the K-line

TABLE 1

SUMMARY OF Ca II AND Mg II OBSERVATIONS

Date	Line	State	Source
1961 May 23..............	Ca II	normal	Griffin (1968)
1963 May 5..............	Ca II	abnormal	Griffin (1963)
1965 March–August.......	Ca II	normal	Liller (1968)
1973 May 19..............	Mg II	abnormal	Moos *et al.* (1974)
1974 April 27..............	Ca II	normal	present work
1974 May 20..............	Mg II	abnormal	McClintock (1975)
1975 January 25...........	Ca II	normal	present work
1975 May 4..............	Ca II	abnormal	present work
1975 December 4..........	Ca II	normal	present work
1976 February 28..........	Ca II	normal?	present work

can be naturally explained by such a chromospheric model. They employed a complete redistribution (CRD) code to compute the line cores and a partial redistribution (PRD) code to compute the inner wings. Since the emission features are chromospheric, we must use for our basic atmospheric model one which includes a chromosphere such as the Ayres-Linsky model. This model yields consistent profiles for the Na D_2 line using a PRD transfer code (Kelch and Milkey 1976). The model of Mäckle *et al.* (1975) contains no chromosphere and is thus not useful for our purpose, and it has been criticized on other grounds (cf. note added in proof to Ayres and Linsky 1975).

As noted above, the abnormal profile differs from the normal profile in that the K_3 central reversal feature is shifted to the blue and the K_{2R} emission peak is brighter than K_{2V}. We will describe these asymmetries by superposing on the basic Ayres and Linsky (1975) Arcturus model a systematic and outward flow of material that is mass-conservative. Preliminary calculations for this problem were described by Linsky *et al.* (1974). In physical terms, the asymmetry results from the increase in outward flow velocity with height (decreasing line optical depth) that is required by the condition that mass flux is conserved, given the decrease of density with height. The effect is to blueshift the K_3 feature, which is relatively dark due to the low value of the surface source function, and to partly absorb the emission from below which constitutes the K_{2V} emission feature.

We have computed a grid of theoretical profiles for the Ca II K- and Mg II k-lines for different values of mass loss, assuming two-level model atoms, plane-parallel atmospheres, and CRD. The transfer equation was solved in the observer's frame using a code based on Rybicki's (1971) modification of the Feautrier (1964) method. We included Voigt profiles with radiative and van der Waals damping and used 50 depth and 27 frequency points. The model chromosphere, microturbulent velocity distribution, and atomic parameters are those of Ayres and Linsky (1975), and the grid is parametrized in units of $M_\odot$ yr^{-1}.

The computed Ca II and Mg II profiles are given in Figures 5, 6, and 7. The integrated intensities have been renormalized to the static profile in order to better visualize the effects of atmospheric expansion. We note the systematic trend of increasing K_3 and k_3 blueshift and increasing $I(K_{2R})/I(K_{2V})$ and $I(k_{2R})/I(k_{2V})$ with increasing mass loss. In Figures 5 and 6, several of the computed profiles have been degraded by the instrumental resolution (0.096 Å for Ca II and 0.4 Å for Mg II) and compared with the observed profiles. We conclude that the abnormal profiles correspond to a mass loss of about 8×10^{-9} $M_\odot$ yr^{-1}, whereas the normal profiles probably limit the mass loss visible in this way to less than 1×10^{-9} $M_\odot$ yr^{-1}. Indeed, the normal profile shows $I(K_{2R}) < I(K_{2V})$ and K_3 shifted slightly to the red, indicative of infalling material. For the larger mass loss rate, the outward flow is about 13 km s^{-1} at Ca II line center ($\tau_K = 1$) and 16 km s^{-1} at Mg II line center ($\tau_k = 1$). Since these optical depths occur at temperatures near 8000 K, the outward flow is supersonic, as the sound speed is 9 km s^{-1}. Note that the primary effect of mass loss on the profiles is to shift the line center in wavelength and to increase $I(K_{2R})/I(K_{2V})$ and $I(k_{2R})/I(k_{2V})$; but the emission peaks are *not* shifted in wavelength. The observed profiles are somewhat broader, and K_3 is not as deep as the computed profiles. These differences can be simply explained by macroturbulence and do not affect the mass
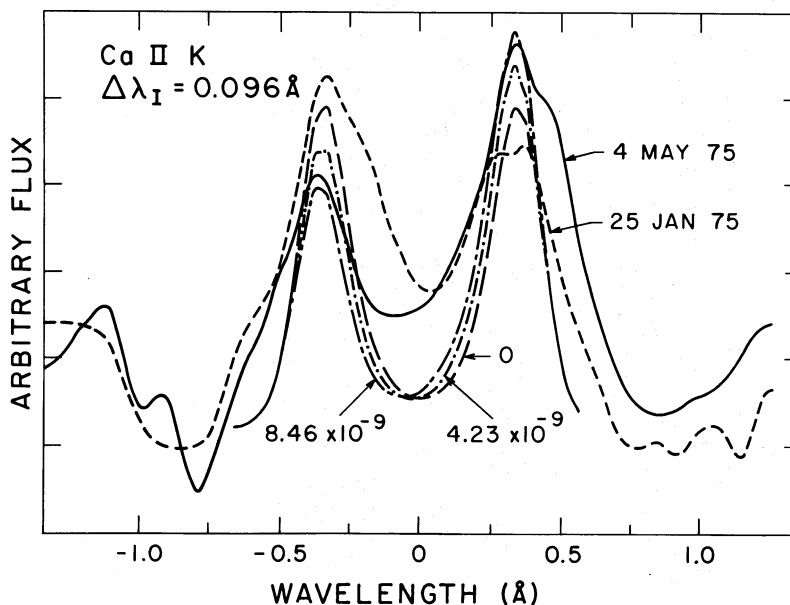

Fig. 6.—Computed Ca II K-line profiles smoothed to an instrumental resolution of 0.096 Å. Profiles are computed for mass loss of 0, 4.23, and 8.46 $\times 10^{-9}$ $M_\odot$ yr^{-1}. Also given are the observed normal profile of 1975 January 25 and observed abnormal profile of 1975 May 4. The neglect of macroturbulence in the calculations may account for the slightly broader profiles and raised K_3 emission in the data.
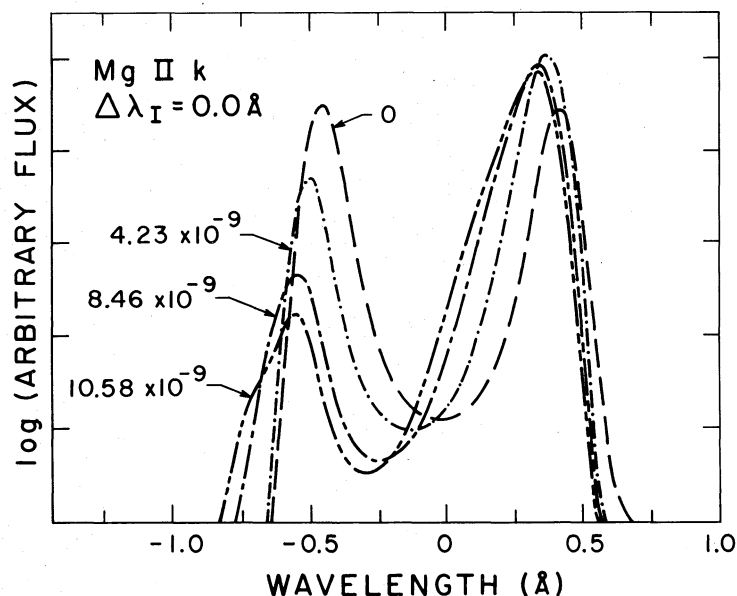
Fig. 7.—Computed intrinsic Mg II k-line profiles. Profiles are computed for mass loss of 0, 4.23, 8.46, and 10.58 $M_\odot$ yr^{-1}.

loss estimates. As we later suggest, large-scale convective activity may be very pronounced in α Boo, and this macroturbulence should be important.

In a subsequent paper we will recompute the profile grid using a comoving frame formulation (cf. Noerdlinger and Rybicki 1974) and PRD, and compare these calculations with additional satellite data. We feel that the present calculations are sufficiently accurate to yield at least a factor of 2 estimate of the mass loss for the given atmospheric model. This statement is based on the considerations that (1) the maximum flow velocity at the level where the optical depth is one in the line center is approximately equal to the local Doppler half-width; (2) we accurately reproduce the Cannon and Vardavas test case described by Mihalas et al. (1976); and (3) we also reproduce the low-velocity test case described in Noerdlinger and Rybicki (1974). Preliminary calculations with the CRD comoving frame formulations do not differ appreciably from those in this paper.

VI. DISCUSSION

Our computed mass loss rates for Arcturus can be compared with estimated mass loss rates derived on theoretical and empirical grounds. Hearn (1975) has derived a general expression for mass loss assuming an isothermal corona. For the stellar parameters of Ayres and Linsky (1975), this expression gives a mass loss of $1–2 \times 10^{-10} M_\odot$ yr^{-1} for $1.6 \times 10^5 \le T_{cor} \le 9 \times 10^6$ K and $<1 \times 10^{-10} M_\odot$ yr^{-1} for $T_{cor} < 1.6 \times 10^5$ K. Reimers's (1975) empirical mass loss relation leads to a mass loss of $1 \times 10^{-9} M_\odot$ yr^{-1} for the Ayres and Linsky stellar parameters and $4 \times 10^{-9} M_\odot$ yr^{-1} for the Mäckle et al. (1975) stellar parameters. However, estimates based on this empirical relation should be viewed with skepticism, since it is derived

from data on M stars and supergiants, whereas Arcturus is a K giant. Finally, we note that Cruddace et al. (1975) estimate upper limits for the mass loss based on their measured upper limits of the soft X-ray flux from Arcturus. Their upper limits are 4×10^{-10} and $1 \times 10^{-10} M_\odot$ yr^{-1} for assumed coronal temperatures of 2.5×10^5 and 1.0×10^6 K, respectively.

From this we conclude that our upper limit estimate of $1 \times 10^{-9} M_\odot$ yr^{-1} for the normal mass loss of Arcturus is consistent with other estimates based on independent lines of evidence. On the other hand, our mass loss estimate of $8 \times 10^{-9} M_\odot$ yr^{-1} for the abnormal Ca II and Mg II profiles clearly refers to an unusual and probably transitory state of the star.

These results on Arcturus are consistent with and may relate to some of the following phenomena in late-type stars.

1. Schwarzschild (1975) suggested as an extreme hypothesis that the characteristic scale for convection in cool supergiants may be a significant fraction of a stellar radius, in which case only a few (~ 10) granules would be present in a given hemisphere of such a star at any one time. Since the mean temperature in the visible photosphere of a granule should differ considerably ($\sim 10^3$ K) depending on whether it is rising or falling, he proposes that the combined effect of the time evolution of the few granules on the visible hemispheres of these stars may account for the irregular variability of their photospheres. In the Sun, it is thought that photospheric convective motions generate acoustic or other wave motions that propagate upward to heat the chromosphere and supply the energy to drive the solar wind. If a similar process is at work in late-type stars as has been suggested by many authors (e.g., Ulmschneider 1967), then the chromospheric heating and mass loss should vary irregularly with time. It is likely that the atmospheric structure and

luminosity of Mira variables, for example, are strongly affected by shocks (Willson 1976).

Arcturus is intermediate in size and luminosity between the supergiants discussed by Schwarzschild and the Sun. As a result, the number of photospheric granules on the visible surface may be of order 10^3 and the variations in the visible broad-band flux may be too small to measure. In the chromospheric spectrum of the Sun, however, the dominant convective cell structures are supergranules of which about 10^2 typically cover the disk. We might expect, moreover, that the disk of a K giant like Arcturus might contain only a few such supergranules. We therefore suggest as an extreme hypothesis that the nonperiodic and large amplitude changes in the Arcturus K-line and, in particular, the abnormal profile of 1975 May 4, may indicate a rapidly rising supergranule near disk center. Simultaneous observations of the Ca II lines with other chromospheric diagnostics such as the Mg II, Lα, and other ultraviolet emission lines would be important in verifying this suggestion, and such observations are under way (Maran et al. 1976). If this explanation is valid, then mass loss rates derived from spectroscopic observations of late-type stars at one time may not represent the time-averaged mass loss.

2. In describing qualitatively the general behavior of the Arcturus H and K double emission peaks in 77 Mount Wilson spectrograms, Griffin (1963) states that the "shortward component of the emission pairs is more variable than the redward component." This behavior can be understood on the assumption, as suggested here, that a major component of the Ca II line variations is due to variable mass loss, so that the variability of K_{2V} is due to changes in the velocity of the blueshifted K_3 absorption feature.

3. Griffin (1963) also notes that on 1961 May 23 the red emission peaks of H and K were weaker than the blue peaks, but on 1963 May 5 the reverse occurred. We feel that this is another example of the phenomenon we are describing. On the other hand, Liller (1968) did not observe a change in sign in $I(K_{2V})/I(K_{2R})$ over an observing period lasting 160 days. This could be due in part to the low resolution (0.35 Å) of his data.

4. Liller (1968) has shown that the variations in the emission peak intensity $I(K_{2R})$ and $I(K_{2V})$ are poorly, if at all, correlated. If the chromospheric physical properties of Arcturus such as the density and temperature distribution (but not the systemic velocity) were to vary with time, then one would expect $I(K_{2R})$ and $I(K_{2V})$ to vary in unison. That the contrary is observed may constitute additional evidence that the primary cause of K-line variations in Arcturus is variable mass loss. A suitable test of this hypothesis would be to search for an inverse correlation of $I(K_{2V})$ with $I(K_{2R})$ and a positive correlation of $\Delta\lambda(K_3)$ with $I(K_{2V})/I(K_{2R})$ in a large sample of data.

5. Griffin (1963) and Liller (1968) both note that the separation of the K_2 peaks and the Wilson-Bappu width of the K-line do not change despite time variations in $I(K_{2R})$ and $I(K_{2V})$. These observations are also consistent with the variable wind explanation (cf. Fig. 4) as the K_2 peaks are formed deep in the chromosphere (Ayres and Linsky 1975) and the Wilson-Bappu width is possibly determined by the location in mass-column density of the temperature minimum (Ayres, Linsky, and Shine 1975). Both features are formed at sufficiently high density that the local stellar wind speed is small compared to the K_3 Doppler shift we measure.

In conclusion, the time behavior of mass loss in late-type stars can now be profitably studied using high-resolution observations of the Ca II and Mg II resonance lines, since the necessary diagnostic techniques are available. As a result, this problem should be vigorously pursued.

REFERENCES

Ayres, T. R., and Linsky, J. L. 1975, Ap. J., 200, 660.
Ayres, T. R., Linsky, J. L., and Shine, R. A. 1975, Ap. J. (Letters), 195, L121.
Brault, J., and Testerman, L. 1972, Kitt Peak Solar Atlas (preliminary ed.; Tucson: Kitt Peak National Observatory).
Buchholz, V., Walker, G. A. H., Auman, J. R., and Isherwood, B. 1973, in Astronomical Observations with Television-Type Sensors, ed. J. W. Glaspey and G. A. H. Walker (Vancouver: Institute of Astronomy and Space Science, U.B.C.), p. 199.
Chiu, H.-Y. 1967, Appl. Optics, submitted.
Chiu, H.-Y., Maran, S. P., Hobbs, R. W., Harris, G. D., Gull, T. R., and Shore, S. N. 1973, in Astronomical Observations with Television-Type Sensors, ed. J. W. Glaspey and G. A. H. Walker (Vancouver: Institute of Astronomy and Space Science, U.B.C.), p. 237.
Cruddace, R., Bowyer, S., Malina, R., Margon, B., and Lampton, M. 1975, Ap. J. (Letters), 202, L9.
Fahlman, G. G., Glaspey, J. W., Jensen, O., Walker, G. A. H.,
and Auman, J. R. 1974, in Planets, Stars and Nebulae Studied with Photopolarimetry, ed. T. Gehrels (Tucson: University of Arizona Press), p. 237.
Feautrier, P. 1964, C.R. Acad. Sci., Paris, 258, 3189.
Griffin, R. F. 1963, Observatory, 83, 255.
———. 1968, A Photometric Atlas of the Spectrum of Arcturus (Cambridge, England: Cambridge Philosophical Society).
Gull, T. R., Goad, L., Chiu, H.-Y., Maran, S. P., and Hobbs, R. W. 1973, Pub. A.S.P., 85, 526.
Hearn, A. G. 1975, Astr. Ap., 40, 355.
Kelch, W. L., and Milkey, R. W. 1976, Ap. J., in press.
Liller, W. 1968, Ap. J., 151, 589.
Linsky, J. L., Basri, G., McClintock, W., Henry, R. C., and Moos, H. W. 1974, Bull. AAS, 6, 458.
Livingston, W. C., and Lynds, C. R. 1964, Ap. J., 140, 818.
Lowrance, J. L., Morton, D. C., Zucchino, P., Oke, J. B., and Schmidt, M. 1972, Ap. J., 171, 233.
Mäckle, R., Holweger, H., Griffin, R. F., and Griffin, R. E. M. 1975, Astr. Ap., 38, 239.

Maran, S. P., Chiu, H. Y., Linsky, J. L., Henry, R. C., Moos, H. W., McClintock, W., and Basri, G. S. 1976, *Bull. AAS*, **8**, 353.
McClintock, W. 1975, private communication.
McClintock, W., Linsky, J. L., Henry, R. C., Moos, H. W., and Gerola, H. 1975, *Ap. J.*, **202**, 165.
Mihalas, D. 1970, *Stellar Atmospheres* (San Francisco: Freeman), p. 372.
Mihalas, D., Shine, R. A., Kunasz, P. B., and Hummer, D. G. 1976, *Ap. J.*, **205**, 492.
Moos, H. W., Linsky, J. L., Henry, R. C., and McClintock, W. 1974, *Ap. J. (Letters)*, **188**, L93.

Morton, D. C., and Richstone, D. O. 1973, *Ap. J.*, **184**, 65.
Morton, W. A., and Morton, D. C. 1972, *Ap. J.*, **178**, 607.
Noerdlinger, P. D., and Rybicki, G. B. 1974, *Ap. J.*, **193**, 651.
Pierce, A. K. 1964, *Appl. Optics*, **3**, 1337.
Reimers, D. 1975, in *Problems in Stellar Atmospheres and Envelopes*, ed. B. Baschek, W. H. Kegel, and G. Traving (New York: Springer-Verlag), p. 229.
Rybicki, G. B. 1971, *J. Quant. Spectrosc. Rad. Transf.*, **11**, 589.
Schwarzschild, M. 1975, *Ap. J.*, **195**, 137.
Ulmschneider, P. 1976, *Zs. f. Ap.*, **67**, 193.
Willson, L. A. 1976, *Ap. J.*, **205**, 172.

P. J. ADAMS and H.-Y. CHIU: Goddard Institute for Space Studies, New York, NY   10025

G. S. BASRI and J. L. LINSKY: Joint Institute for Laboratory Astrophysics, University of Colorado, Boulder, CO   80309

R. W. HOBBS and S. P. MARAN: Laboratory for Solar Physics and Astrophysics, NASA Goddard Space Flight Center, Greenbelt, MD   20771